QUANTUM MECHANICS

Quantum mechanical double slit for molecular scattering

Haowen Zhou, William E. Perreault, Nandini Mukherjee*, Richard N. Zare*

Interference observed in a double-slit experiment most conclusively demonstrates the wave properties of particles. We construct a quantum mechanical double-slit interferometer by rovibrationally exciting molecular deuterium (D_2) in a biaxial ($v = 2, j = 2$) state using Stark-induced adiabatic Raman passage, where v and j represent the vibrational and rotational quantum numbers, respectively. In D_2 ($v = 2, j = 2$) → D_2 ($v = 2, j' = 0$) rotational relaxation via a cold collision with ground state helium, the two coherently coupled bond axis orientations in the biaxial state act as two slits that generate two indistinguishable quantum mechanical pathways connecting initial and final states of the colliding system. The interference disappears when we decouple the two orientations of the bond axis by separately constructing the uniaxial states of D_2, unequivocally establishing the double-slit action of the biaxial state. This double slit opens new possibilities in the coherent control of molecular collisions.

Studying the underlying quantum principles that drive all molecular interactions will promote our ability to manipulate the microscopic world, with potential applications ranging from molecular engineering to the realization of a quantum computer. At the heart of quantum mechanics lies the uncertainty principle, which discards the classical idea of localization, thereby introducing the wave property of matter. As a direct consequence of the wave nature of matter, interactions at the quantum scale are often controlled by interference of indistinguishable quantum mechanical pathways connecting initial and final states (*1*). The importance of this property extends all the way to biology, where interference between quantum mechanical pathways makes possible highly efficient energy transport from chromophores to the photosynthetic reaction center (*2*). We describe here the fabrication of a molecular interferometer that uses the fundamental wave character of quantum systems to interrogate and control molecular collision processes.

One of the earliest and most fundamental demonstrations of quantum mechanical interference was Young's original double-slit experiment with optical waves. Following this, a long series of experiments have been designed that use monoenergetic beams of particles ranging in mass from electrons to large molecules to show matter-wave interferences when the particles pass through two mechanical slits (*3*–*6*). These interferences only appear when the transverse coherence is maintained across both slits either by using a sufficiently large De Broglie wavelength or by restricting the size of the slit that admits the particle beam into the double-slit interferometer. More recently, double-slit interference has been realized in unimolecular and bimolecular scattering by using the two atomic centers of a diatomic molecule, which are the natural double slits of the quantum world (*7*–*10*). Although these experiments have culminated in the successful realization of the Bohr-Einstein recoiling double-slit thought experiment (*8*, *11*), the naturally occurring double slits cannot be used to actively control a molecular process. Instead, we use specially prepared quantum states to construct a double slit, which advances the coherent control of molecular scattering.

Stimulated by the recent interest in quantum science, there has been an upsurge of experimental (*12*–*18*) and theoretical (*19*–*24*) investigations on the control of molecular processes using interferences between coherently prepared quantum states. Many molecular scattering experiments have observed quantum interference that results from the material properties of the system without achieving control (*25*–*32*). On the other hand, our earlier cold scattering experiments (*16*–*18*) achieved steric control by aligning the molecules using Stark-induced adiabatic Raman passage (SARP) (*33*, *34*) by choosing different polarizations of the pump and Stokes lasers (*35*). Each of these alignments can be expressed as a superposition of the magnetic sublevels within a rovibrational energy state, and so the measured scattering distribution results from interference between different sublevels. Others have performed similar experiments, including, for example, Nichols *et al.* (*12*), who studied orientational effects in inelastic collision by aligning the NO molecules using a dc field. Alignment in a strong electric field produced a coherent mixture of the even and odd Λ- doublet states, which created interference effects in the output of the scattering process. However, each of these superpositions did not form a double slit because, with a suitable choice of the basis set, it could be converted to a single quantum state (uniaxial system). We achieve a double-slit interference in a two-body collision by creating coherent coupling between two orthogonal states of one of the collision partners.

Specifically, we studied the rotational relaxation of aligned D_2 ($v = 2, j = 2$) → D_2 ($v = 2, j' = 0$) at a single collision level, mediated by a ground state He atom within a cold supersonically expanded mixed molecular beam, where v and j represent the vibrational and rotational quantum numbers, respectively. SARP is able to transfer nearly the complete ground state population of D_2 to the rovibrational energy eigenstate ($v = 2, j = 2$) (*36*) with its bond axis prepared in a biaxial orientation in the laboratory frame (*35*). The biaxial state coherently couples two orientations of the D_2 bond axis, meaning that the molecule simultaneously exists in two possible orientations, and so no coordinate transformation can convert it to a pure state. As such, the density matrix for this state cannot be diagonalized by any unitary transformation. Thus, defining this nonclassical state requires the phase coherence information represented by the nonzero off-diagonal density matrix in addition to population information. The two orientations generate two quantum mechanical pathways in the rotationally inelastic collision that interfere to produce a strong modulation in the scattering intensity distribution. As such, scattering from the coupled orientations of the biaxial state mimics the way that a photon or particle simultaneously experiences the two mechanical slits in a traditional double-slit scattering experiment. Our earlier theoretical study (*37*) showed that the biaxial state is capable of producing an interference pattern in the scattering intensity in the plane perpendicular to the collision velocity. In this study, we experimentally demonstrate the double-slit action and show that the interference is evident in the scattering distribution projected parallel to the collision velocity. To establish unequivocally the double-slit action of the biaxial state, we show that the strong modulation in the scattering intensity distribution disappears when the contributions from the two orientations are considered independently, just as the interference pattern disappears in a traditional double slit by blocking one of the slits. Thus, our experiment not only illustrates the ability of quantum interference to control a molecular collision but also shows that the biaxial state is a purely quantum mechanical object that has a one-to-one correspondence with a double slit.

Experimental demonstration of a molecular double slit

To study cold collisions with SARP-prepared uniaxial and biaxial states, we expanded a mixture of D_2 and He (ratio 1:10) in a single supersonic beam using an Even-Lavie pulsed valve (*38*). The supersonically expanded and collimated beam (divergence ≤12 mrad) not only dramatically reduced the collision temperature (~1 K) (*39*) but also defined a direction with respect to which the D_2 bond axis is aligned

Department of Chemistry, Stanford University, Stanford, CA 94305, USA.
*Corresponding author. Email: nmukherj@stanford.edu (N.M.); zare@stanford.edu (R.N.Z.)

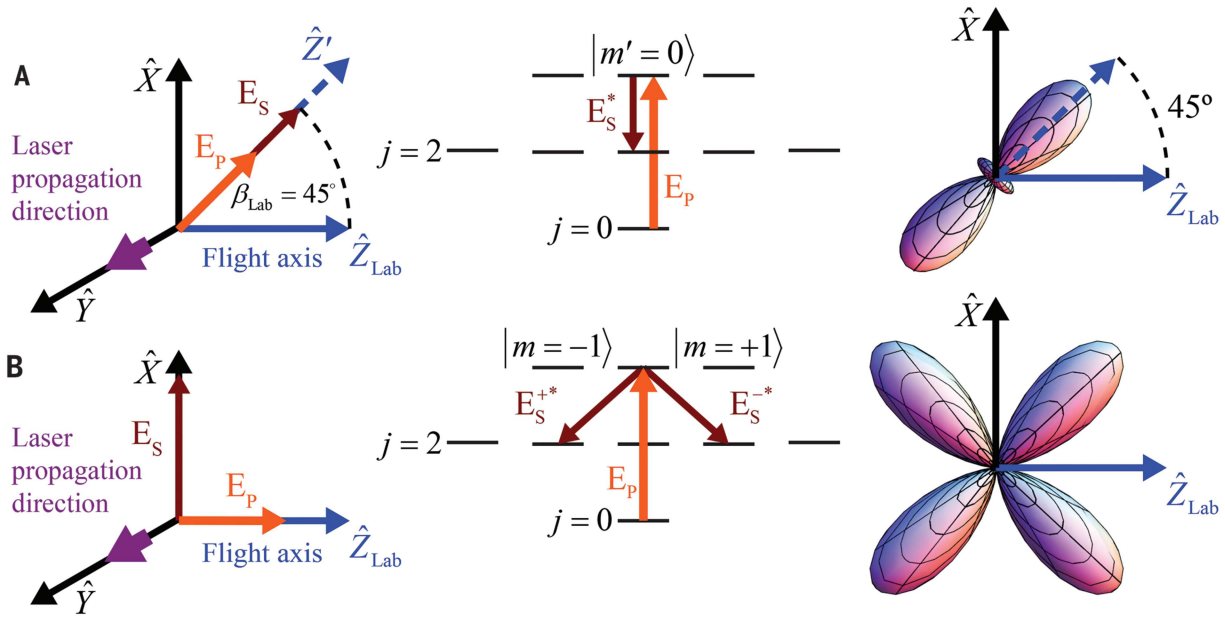

Fig. 1. SARP preparation of uniaxial and biaxial states of D_2 (v = 2, j = 2) by combining different polarizations of the pump and Stokes laser pulses. (**A**) SARP preparation of D_2 (v = 2, j = 2) with bond axis aligned at $\beta_{Lab} = \pi/4$ relative to the lab-fixed axis Z_{Lab} oriented along the molecular beam axis, which is also the flight axis of the detected ions. This alignment was achieved using parallel pump and Stokes linear polarizations along Z' oriented at 45° relative to Z_{Lab}. The quantum number m' refers to the projection of the j = 2 angular momentum vector along the quantization axis Z'. (**B**) SARP preparation of the biaxial state with cross-polarized pump (along Z_{Lab}) and Stokes (along X) laser pulses. The m quantum number refers to the projection of the j = 2 angular momentum vector along the quantization axis Z_{Lab}. In both schematics, E_P refers to the absorption of a pump photon, and E_S^* refers to the emission of a Stokes photon in a lambda-type transition. On the right, we display the three-dimensional molecular axis distributions for the prepared states of D_2.

using SARP. Using resonance-enhanced multiphoton ionization (REMPI), we determined that ~40% of the D_2 (v = 0) population in the mixed supersonic beam was in the j = 0 state, with the remainder distributed among the j = 1, 2, and 3 states. To prepare the uniaxial and biaxial states of D_2, we intersected the D_2-He mixed molecular beam transversely with a sequence of pump and Stokes laser pulses partially overlapping in time. A comprehensive description of SARP can be found elsewhere (*34*). The SARP preparation process is able to transfer nearly 100% of the D_2 (v = 0, j = 0) population to the target D_2 (v = 2, j = 2) state (*36*). After SARP preparation, the D_2 molecules collided with He atoms and relaxed to the (v = 2, j' = 0) state, where they were state-selectively ionized using REMPI.

The orientation of the molecular bond axis was controlled using the polarization directions of the pump and Stokes laser pulses and is defined relative to a lab-fixed frame with coordinate axes X, Y, and Z_{Lab}. Figure 1 describes the experimental arrangement and gives a schematic of SARP excitation to prepare the uniaxial (Fig. 1A) and biaxial (Fig. 1B) states. Figure 1A shows the preparation of D_2 (v = 2, j = 2) with its bond axis oriented at $\beta_{Lab} = \pi/4$ relative to Z_{Lab} using pump and Stokes fields with polarization along $\beta_{Lab} = \pi/4$. In a similar way, D_2 (v = 2, j = 2) can be prepared with its bond axis aligned at $\beta_{Lab} = -\pi/4$ relative to Z_{Lab} using pump and Stokes laser polarizations along $\beta_{Lab} = -\pi/4$ (not shown). We call the wave functions of the two uniaxial states with the bond axis aligned at $\beta_{Lab} = \pi/4$ and $\beta_{Lab} = -\pi/4$ as ψ_+ and ψ_-, respectively. Figure 1B shows the preparation of a biaxial state using SARP with a cross-polarized pump and Stokes laser fields. This state is called XSARP, and its wave function is denoted by ψ_X. We note that biaxial and multiaxial atomic states have been prepared for use in scattering experiments previously (*40*, *41*), but this work did not examine interference effects as we will do here.

Using the angular momentum representation in terms of m, the projection quantum number of the angular momentum vector $\boldsymbol{j}$ on the quantization axis Z_{Lab}, the wave functions of the two uniaxial states ψ_+ and ψ_- are expressed as

$$\psi_\pm = 0.25|m=0\rangle \pm 0.612[|m=-1\rangle - |m=+1\rangle] + 0.306[|m=+2\rangle + |m=-2\rangle] \quad (1)$$

In the same representation, the XSARP can be expressed as

$$\psi_X = (|m=+1\rangle - |m=-1\rangle)/\sqrt{2} \quad (2)$$

The three states, $\psi_\pm$ and ψ_X are defined with respect to the same quantization axis Z_{Lab}. Using Eqs. 1 and 2, ψ_X can be written as a superposition of the two uniaxial states $\psi_\pm$:

$$\psi_X = 0.577[|\psi_+\rangle - |\psi_-\rangle] \quad (3)$$

The biaxial state ψ_X thus coherently ties the two axes of the uniaxial states ψ_+ and ψ_-. The data we present here show that this phase coherence causes a strong modulation in the intensity distribution of the scattered D_2 (v = 2, j' = 0) in the same fashion as a double slit causes interference fringes.

The double-slit interference effect in the scattering of the biaxial state can be readily seen in the expression for the center-of-mass-frame angular distribution for the XSARP state. For the biaxial XSARP state in Eq. 3, each rotationally inelastic collision is mediated by the D_2 bond axis simultaneously occupying two alignments at $\beta_{Lab} = \pi/4$ and $\beta_{Lab} = -\pi/4$. The scattering intensity distribution as a function of the polar angle θ is obtained by integrating over the azimuthal angle φ. The scattering intensity for ψ_X is thus

$$I_X(\theta) = \sin\theta \left[\int_0^{2\pi} |f_X(\theta,\varphi)|^2 d\varphi\right] \quad (4)$$

where f_X represents the scattering amplitude for D_2 prepared in the initial state

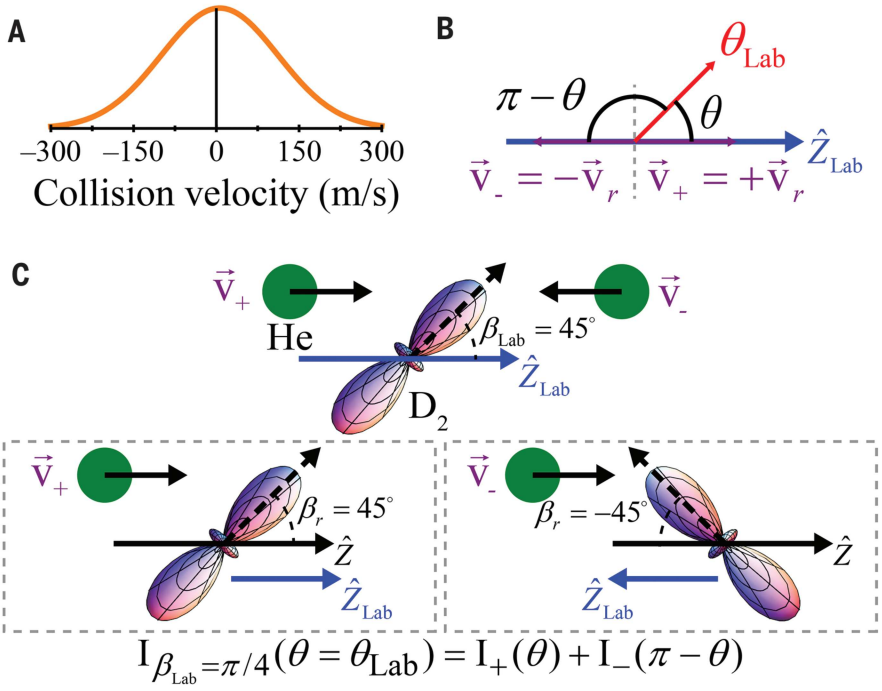

Fig. 2. Effect of the symmetric collision velocity distribution on the scattering measurement. (**A**) Experimentally determined collision velocity distribution for the D_2-He scattering in the mixed molecular beams. (**B**) Schematic representation of the conversion of center-of-mass-frame scattering angle to lab-frame scattering angle for the positive ($\vec{v}_+$) and negative ($\vec{v}_-$) velocities relative to Z_{Lab}. (**C**) Schematic demonstration that for the $\beta_{Lab} = \pi/4$ preparation, the $\vec{v}_+$ velocity group sees a center-of-mass orientation $\beta_r = \pi/4$, whereas the $\vec{v}_-$ velocity group sees a center-of-mass orientation $\beta_r = -\pi/4$.

ψ_X. Using the expression of ψ_X in Eq. 3, we can write

$$f_X(\theta,\varphi) = 0.577[f_+(\theta,\varphi) - f_-(\theta,\varphi)] \quad (5)$$

In Eq. 5, f_+ and f_- give the center of mass scattering amplitudes for the initial quantum states prepared in ψ_+ and ψ_-, respectively. Using Eq. 5, the scattering intensity for the biaxial state can be expressed as follows:

$$I_X(\theta) = [I_+(\theta) - I_-(\theta) - I_{Int}(\theta)] \quad (6)$$

where $I_\pm(\theta)$ represents the center-of-mass-frame scattering angular distribution for the initial state prepared in $\psi_\pm$ and is given by

$$I_\pm(\theta) = \sin\theta \int_0^{2\pi} |f_\pm(\theta,\varphi)|^2 d\varphi \quad (7)$$

$I_\pm(\theta)$ gives the contribution of individual axis orientations, or slits, and is entirely determined by the absolute square of the scattering amplitude $f_\pm$. $I_{Int}(\theta)$ gives rise to the double-slit interference

$$I_{Int}(\theta) = \sin\theta \int_0^{2\pi} [f_+(\theta,\varphi) f_-^*(\theta,\varphi) + f_+^*(\theta,\varphi) f_-(\theta,\varphi)] d\varphi \quad (8)$$

and is determined from the relative phase of the scattering amplitudes f_+ and f_-. The interference term arises from coherence between the two bond axis orientations, which is equivalent to the phase correlation between the two slits in the double-slit experiment when the De Broglie wavelength becomes sufficiently large to couple both the slits. This interference manifests itself as strong modulation in the scattering intensity, as we show below.

However, the lab-frame angular distribution that we measure and show below is not the same as the center-of-mass-frame distribution. This is because collisions with both positive ($\vec{v}_+ = \vec{v}_r$) and negative ($\vec{v}_- = -\vec{v}_r$) relative velocities with respect to the $+Z_{Lab}$ axis are present in the symmetric collision velocity distribution shown in Fig. 2A. As a result, the experimentally measured scattering intensity at a lab angle $\theta_{Lab} = \theta$ defined relative to $+Z_{Lab}$, is the sum of the contributions due to scattering at an angle θ from the positive ($\vec{v}_+$) collision velocity and scattering at angle $\pi - \theta$ from the negative ($\vec{v}_-$) collision velocity. As shown in Fig. 2C, for the negative velocity group, the center-of-mass-frame Z axis is flipped with respect to the lab frame. As a result, the bond axis orientation in the center-of-mass frame for the negative collision velocity group is flipped such that $\beta_r = -\beta_{Lab}$. Including the contributions of both collision velocity groups, the lab-frame scattering intensities for the uniaxial states ψ_+ and ψ_- are given by

$$I_{\beta_{Lab}=\pm\pi/4}(\theta=\theta_{Lab}) = I_\pm(\theta) + I_\mp(\pi-\theta) \quad (9)$$

Using Eq. 9, we arrive at the following expression for the lab-frame scattering angular distribution for the biaxial state:

$$I_X(\theta_{Lab}=\theta) = \{I_+(\theta) + I_-(\pi-\theta) + I_-(\theta) + I_+(\pi-\theta) - [I_{Int}(\theta) + I_{Int}(\pi-\theta)]\} = \{I_{\beta_{Lab}=\pi/4}(\theta) + I_{\beta_{Lab}=-\pi/4}(\theta) - [I_{Int}(\theta) + I_{Int}(\pi-\theta)]\} \quad (10)$$

We have used Eqs. 9 and 10 to analyze the experimental angular distribution for the uniaxial and biaxial states shown in Fig. 3. In Eq. 10, the contributions of $I_{\beta_{Lab}=\pm\pi/4}$ represent the transmission of one slit at a time. This contribution is experimentally isolated because we were able to prepare each of the uniaxial states separately, and so we can show explicitly the double-slit interference of the biaxial state that arises from the cross terms $f_+(\theta,\varphi) f_-^*(\theta,\varphi)$ in the expression of I_{Int} (Eq. 8). For the homonuclear symmetry of D_2, we can show analytically that the φ integrated scattering intensities for the two uniaxial states are identical, which we have also verified experimentally. The supplementary materials contain a description of these experiments, as well as a more in-depth derivation of Eqs. 9 and 10.

Figure 3 compares the experimental scattering angular distribution for the uniaxial and biaxial bond axis orientation of D_2 ($v = 2, j = 2$). Our experimental method for measuring scattering angular distributions has been described in detail in an earlier publication (*16*). Figure 3A shows the experimental scattering data obtained using the uniaxial alignment at $\beta_{Lab} = \pi/4$ As we mentioned above and show in detail in the supplementary materials, the scattering angular distribution for $\beta_{Lab} = -\pi/4$ was identical. Figure 3B shows the measured scattering intensity for the biaxial state. Clearly, the double-slit interference that is present in the scattering of the biaxial state produced a strong modulation in the scattering intensity near 90°. Using the scattering matrix for the rotationally inelastic scattering D_2 ($v = 2, j = 2$) → D_2 ($v = 2, j' = 0$), which was determined in our previous experiments, we calculated the scattering intensities using Eqs. 9 and 10 (see supplementary materials for details). The calculated scattering intensity is superimposed on the experimental data shown in Fig. 3 for the uniaxial and biaxial alignments. The strong correspondence between the calculations and our experimental measurements not only demonstrates the double-slit action of the biaxial state but also validates the scattering matrix

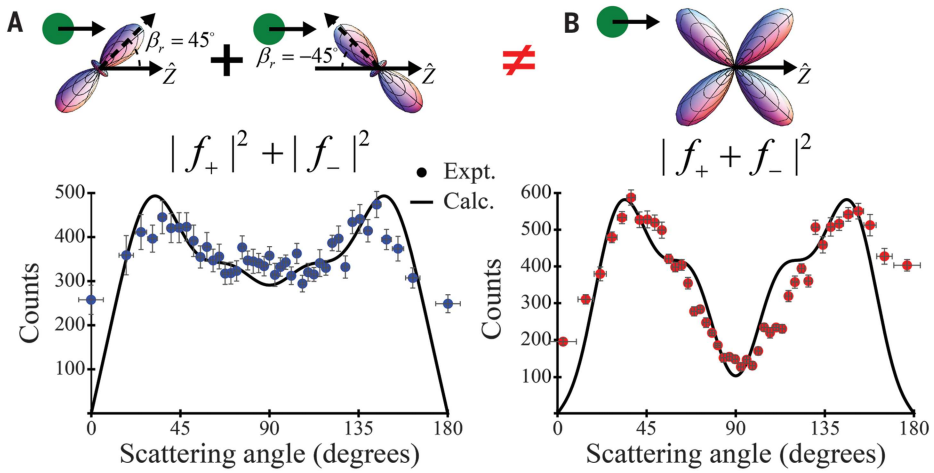

Fig. 3. Demonstration of double slit by preparing biaxial and uniaxial states for the bond axis of D_2 (v = 2, j = 2). For clarity, the top panels only show the collision for the positive collision velocity group. (**A**) Experimental scattering distribution (blue dots) for the uniaxial bond axis orientation at $\beta_{Lab} = \pi/4$. As discussed in the text, this is identical to the distribution measured with the $\beta_{Lab} = -\pi/4$ orientation. (**B**) Experimental scattering distribution (red dots) for the XSARP biaxial bond axis orientation. The black solid lines in (A) and (B) show the calculated angular distribution using the scattering matrix. The vertical error bars represent one standard deviation in the number of counts at a given scattering angle, and the horizontal error bars give the experimental uncertainty in the determination of the scattering angle.

elements that we determined in our earlier work (*15*).

Conclusion

We have created a quantum mechanical double slit by preparing the rovibrationally excited D_2 (v = 2, j = 2) molecule in a biaxial state. The coherently coupled bond axis orientations in the biaxial state lead to two indistinguishable pathways connecting the input state and final state of the Δj = 2 rotationally inelastic D_2-He collision. Therefore, they act as the two slits of a double-slit interferometer. This double-slit interference manifested as a strong modulation in the measured angular distribution of the rotationally relaxed D_2 (v = 2, j' = 0). To prove that the observed interference arose from the double-slit action of the biaxial state, we measured the effect of one slit at a time by separately constructing each of the uniaxial states contained within the biaxial state superposition. Measuring the contributions of the individual slits separately is equivalent to decoupling the axes in the biaxial state. When we add the scattering angular distributions measured for each slit, the result is notably different from that of the biaxial state. This difference that clearly arises from the quantum mechanical interference of the two orientations, which act as the two slits, unequivocally establishes the double-slit action of the biaxial state.

As discussed in the introduction, many previous atomic and molecular scattering experiments have used the quantum mechanical interference of a double slit to interpret their results. Of these, only a few were able to experimentally isolate the double-slit contribution from that of decoupled single slits and thereby demonstrate that interference arises exclusively when the two slits are coupled as we have done here. One elegant example (*11*) examined the interferences present in the Auger spectrum of a core-excited diatomic molecule that arise as a result of two indistinguishable pathways for electron emission when the excited electron is delocalized over the two atomic centers. They showed that the interference disappears when the system is prepared in the dissociative state because it becomes possible to identify which slit (atom) the electron is emitted from. As impressive as these experiments are, there is unfortunately not a straightforward way to use these double slits as a tool to control further scattering processes.

In the present work, we have demonstrated the use of quantum states as slits as opposed to individual atoms. This gives us the ability to use our experimentally engineered molecular quantum interferometer to control or measure the fundamental properties of a molecular process. For example, using our molecular double slit, the relative phases of the scattering matrix elements can be experimentally measured (*42*), which allows a direct test of theoretical calculations on important, fundamental collision processes. In this example, we have demonstrated fabrication of a double slit by coherently coupling the two uniaxial states with a fixed phase relationship. A higher level of control can be obtained by introducing a variable phase relation between the coherently coupled states that can be further manipulated using various optical and electro-optical techniques (*35*). Our ability to coherently control the molecular double slit is not limited to inelastic collisions but is more general, opening completely new possibilities in the control of bimolecular reactions.

REFERENCES AND NOTES

1. R. P. Feynman, R. B. Leighton, M. L. Sands, *Feynman Lectures on Physics, Vol. 3* (Addison Wesley Publishing Co., 1963).
2. G. S. Engel *et al.*, *Nature* **446**, 782–786 (2007).
3. A. H. Tavabi *et al.*, *Sci. Rep.* **9**, 10458 (2019).
4. S. Frabboni, G. C. Gazzadi, G. Pozzi, *Am. J. Phys.* **75**, 1053–1055 (2007).
5. M. Arndt *et al.*, *Nature* **401**, 680–682 (1999).
6. O. Carnal, J. Mlynek, *Phys. Rev. Lett.* **66**, 2689–2692 (1991).
7. D. Misra *et al.*, *Phys. Rev. Lett.* **102**, 153201 (2009).
8. L. P. H. Schmidt *et al.*, *Phys. Rev. Lett.* **111**, 103201 (2013).
9. D. Akoury *et al.*, *Science* **318**, 949–952 (2007).
10. S. E. Canton *et al.*, *Proc. Natl. Acad. Sci. U.S.A.* **108**, 7302–7306 (2011).
11. X. J. Liu *et al.*, *Nat. Photonics* **9**, 120–125 (2015).
12. B. Nichols *et al.*, *Chem. Sci.* **6**, 2202–2210 (2015).
13. M. H. G. de Miranda *et al.*, *Nat. Phys.* **7**, 502–507 (2011).
14. S. D. S. Gordon *et al.*, *Nat. Chem.* **10**, 1190–1195 (2018).
15. H. Zhou, W. E. Perreault, N. Mukherjee, R. N. Zare, *J. Chem. Phys.* **154**, 104309 (2021).
16. W. E. Perreault, N. Mukherjee, R. N. Zare, *Science* **358**, 356–359 (2017).
17. W. E. Perreault, N. Mukherjee, R. N. Zare, *J. Chem. Phys.* **150**, 174301 (2019).
18. W. E. Perreault, N. Mukherjee, R. N. Zare, *Nat. Chem.* **10**, 561–567 (2018).
19. M. Shapiro, P. Brumer, *Phys. Rev. Lett.* **77**, 2574–2576 (1996).
20. A. Devolder, T. Tscherbul, P. Brumer, *Phys. Rev. A* **102**, 031303 (2020).
21. P. Brumer, A. Abrashkevich, M. Shapiro, *Faraday Discuss.* **113**, 291–302 (1999).
22. J. L. Krause, M. Shapiro, P. Brumer, *J. Chem. Phys.* **92**, 1126–1131 (1990).
23. C. A. Arango, M. Shapiro, P. Brumer, *J. Chem. Phys.* **125**, 094315 (2006).
24. P. Král, I. Thanopulos, M. Shapiro, *Rev. Mod. Phys.* **79**, 53–77 (2007).
25. G. Sha, J. He, B. Jiang, C. Zhang, *J. Chem. Phys.* **102**, 2772–2779 (1995).
26. J. Onvlee *et al.*, *Nat. Chem.* **9**, 226–233 (2017).
27. X. L. Chen *et al.*, *Chem. Phys. Lett.* **318**, 107–112 (2000).
28. P. G. Jambrina *et al.*, *Nat. Chem.* **7**, 661–667 (2015).
29. P. G. Jambrina, J. Aldegunde, F. J. Aoiz, M. Sneha, R. N. Zare, *Chem. Sci.* **7**, 642–649 (2016).
30. M. Sneha *et al.*, *J. Chem. Phys.* **145**, 024308 (2016).
31. Y. Xie *et al.*, *Science* **368**, 767–771 (2020).
32. B. K. Kendrick *et al.*, *Phys. Chem. Chem. Phys.* **23**, 5096–5112 (2021).
33. N. Mukherjee, R. N. Zare, *J. Chem. Phys.* **135**, 024201 (2011).
34. N. Mukherjee, W. E. Perreault, R. N. Zare, in *Frontiers and Advances in Molecular Spectroscopy*, J. Laane, Ed. (Elsevier, 2018), pp. 1–46.
35. N. Mukherjee, W. Dong, R. N. Zare, *J. Chem. Phys.* **140**, 074201 (2014).
36. W. E. Perreault, N. Mukherjee, R. N. Zare, *J. Chem. Phys.* **150**, 234201 (2019).
37. W. E. Perreault, H. Zhou, N. Mukherjee, R. N. Zare, *Front. Phys. (Lausanne)* **9**, 671997 (2021).
38. U. Even, *EPJ Tech. Instrum.* **2**, 17 (2015).
39. W. E. Perreault, N. Mukherjee, R. N. Zare, *Chem. Phys.* **514**, 150–153 (2018).
40. R. L. Robinson, L. J. Kovalenko, S. R. Leone, *Phys. Rev. Lett.* **64**, 388–391 (1990).
41. J. P. J. Driessen, C. J. Smith, S. R. Leone, *J. Phys. Chem.* **95**, 8163–8169 (1991).
42. Y. Gao *et al.*, *Phys. Rev. A* **97**, 020701 (2018).
43. H. Zhou, W. E. Perreault, N. Mukherjee, R. N. Zare, Quantum mechanical double slit for molecular scattering. Dataset. Dryad (2021); https://doi.org/10.5061/dryad.jh9w0vtcb.

ACKNOWLEDGMENTS

Funding: This work was supported by the US Army Research Office through the MURI program under grant no. W911NF-19-1-0283 and

the National Science Foundation under grant no. PHY- 2110256.
Author contributions: Experimental data were taken by H.Z., W.E.P., and N.M., and calculations were performed by N.M. All authors participated in discussion and writing of the manuscript. **Competing interests:** None declared. **Data and materials availability:** All data needed to evaluate the conclusions in this paper are present in the paper or supplementary materials. All data presented in this paper are deposited at Dryad (*43*).

SUPPLEMENTARY MATERIALS

science.org/doi/10.1126/science.abl4143
Materials and Methods
Supplementary Text
Figs. S1 and S2
Table S1
References (*44*, *45*)

12 July 2021; accepted 23 September 2021
10.1126/science.abl4143

Science

Quantum mechanical double slit for molecular scattering

Haowen ZhouWilliam E. PerreaultNandini MukherjeeRichard N. Zare

Science, 374 (6570), • DOI: 10.1126/science.abl4143

Double slits with molecular states

Despite decades of research, the role of quantum mechanical effects in molecular scattering has not yet been fully investigated and can still demonstrate fascinating results, even for simple triatomic systems. Zhou *et al*. show that the entangled bond axis orientations in the biaxial state of a deuterium molecule can act as the two slits of a double-slit interferometer for rotationally inelastic collision with a helium atom, giving rise to quantum interference between two indistinguishable pathways (see the Perspective by Wang and Yang). The present work presents an elegant example of quantum interference in molecular scattering that is conceptually similar to the famous Young's optical double-slit experiment. The proposed molecular interferometer could be used to coherently control the phases in various molecular processes in future experiments. —YS

Science (ISSN) is published by the American Association for the Advancement of Science. 1200 New York Avenue NW, Washington, DC 20005. The title *Science* is a registered trademark of AAAS.